Molecular Catalysis 462 (2019) 69–76

Contents lists available at ScienceDirect

Molecular Catalysis

journal homepage: www.elsevier.com/locate/mcat

Selective hydrogenolysis of lignin and model compounds to monophenols over $AuPd/CeO_2$

Xiaoqing Gao[a,b], Shanhui Zhu[a,*], Yongwang Li[a,b]

[a] State Key Laboratory of Coal Conversion, Institute of Coal Chemistry, Chinese Academy of Sciences, Taiyuan 030001, PR China
[b] Synfuels China Co. Ltd., Beijing 100195, PR China

ARTICLE INFO

Keywords:
Lignin
Model compounds
Hydrogenolysis
Au
Pd

ABSTRACT

The mild depolymerization of lignin into aromatic monomer is a grand challenge owing to the various aryl ether C–O bonds, particularly for the most abundant β-O-4, α-O-4 and 4-O-5 linkages. Rod-shaped CeO_2 supported AuPd bimetallic catalysts fabricated by sol-immobilization method presented robust alloy structure, as evidenced by TEM, XPS, UV–vis, and CO-DRIFTS. For the hydrogenolysis of C—O bond model compound with formic acid, Au_1Pd_1/CeO_2 showed about 23.5 and 6 folds increase in activity compared with its monometallic counterparts Au/CeO_2 and Pd/CeO_2, respectively. The outstanding performance was mainly ascribed to the increased adsorption ability of electron-deficient Pd for aromatic C–O bond. Additionally, formic acid-mediated Au_1Pd_1/CeO_2 has efficiently performed hydrogenolysis of real lignin into a variety of valuable monophenols, achieving 44.1% yield at low temperature.

1. Introduction

The transformation of renewable lignocellulosic biomass into high-value chemicals and liquid fuels has stimulated intensive interests with the increasing energy demand and decreasing fossil resources. Lignin is the second most abundant carbon-containing resource on earth after cellulose, and the only sustainable source for aromatic chemicals [1,2]. Owing to the recalcitrant and complex molecular structure, lignin is generally regarded as a waste product, or directly burned to supply energy. These behaviours seriously cause environmental pollution and lose a potentially versatile raw material [3,4]. Therefore, it is urgent to develop new processes to transform low-cost lignin into value-added chemicals. In this context, hydrogenolysis of lignin to aromatic monophenols is one of the most promising methods owing to their wide applications as intermediates in the synthesis of fine chemicals or bio-oils [1].

The lignin polymer is composed of methoxy-substituted phenolic subunits that are connected through many different types of linkages (Scheme 1) [1,2]. The three of most abundant structural motifs is β-O-4, α-O-4 and 4-O-5 linkages, which accounts for 45–62%, 3–12% and 4–9% of the aryl ether C–O bonds in hardwoods lignin, respectively. It is a grand challenge to activate and break these aryl ether C–O bonds under mild conditions owing to its high cleavage energy (218-314 kJ mol^{-1}). Recently, some simple dimer model chemicals have been utilized to explore the cleavage mechanism for the aryl ether C–O bonds in lignin depolymerization [5–10], because more complex substitutions hardly affect the principal chemistry. Homogenous catalysts Ni [11], Ru [12] and Fe [13] complexes have demonstrated to be active and efficient to exclusively cleave aryl ether C–O bonds under low temperature and H_2 pressure. However, the inherent deficiency of homogenous system limits their large-scale applications. Therefore, a variety of heterogeneous catalysts such as supported Ni [5,6,14–16], Ru [17], Pd [18], Pt [9] and Fe [19] have been attempted to perform hydrogenolysis of aryl ether C–O bonds to produce aromatics in the presence of high pressure H_2. Lercher. et al. [5] employed benzyl phenyl ether (α-O-4 linkage), 2-phenylethyl phenyl ether (β-O-4 linkage), and diphenyl ether (4-O-5 linkage) to mimic various C–O bonds of lignin. The selective hydrogenolysis of these model compounds produces aromatic phenols, cycloalkanes and cyclohexanol over Ni/SiO_2 in aqueous solution, and the cleavage rate for C–O bond declines in the sequence of α-O-4, 4-O-5 and β-O-4. Abu-Omar et al. [18] describes a PdZn/C catalyst for selective cleavage β-O-4 linkages of lignin model substrate with 85% yield in 2 MPa H_2 using methanol as solvent. Moreover, this catalyst efficiently converts lignin into monophenols at 250 °C in yields of 19–54% depending on the source of lignin.

Very recently, many bimetallic catalysts, such as NiAu [10], NiRu [8], NiRh [8], NiPd [8], PdFe [20,21], PdNi [22] and CoMo [23] have been effectively applied for hydrogenolysis of C–O bond of lignin and

* Corresponding author.
E-mail address: zhushanhui@sxicc.ac.cn (S. Zhu).

https://doi.org/10.1016/j.mcat.2018.10.022
Received 20 July 2018; Received in revised form 27 October 2018; Accepted 30 October 2018

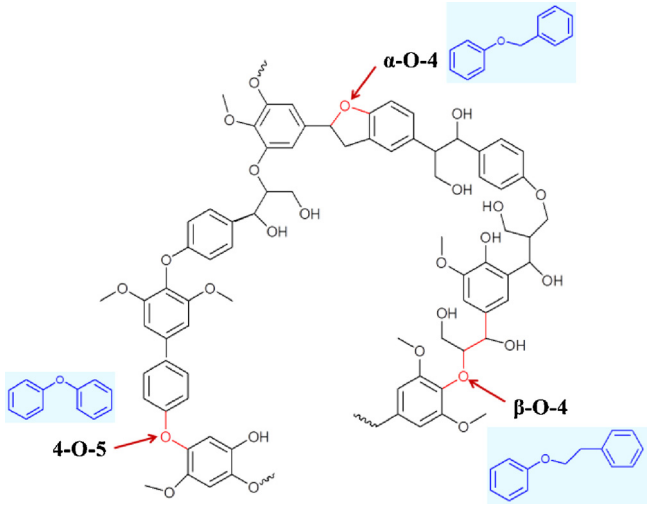

Scheme 1. Fragment structure of lignin and corresponding model compounds.

its model chemicals, because they are remarkably active and stable than their equivalent monometallic catalysts. Yan et al. [10] developed a highly active NiAu for the hydrogenolysis of β-O-4 bond at low temperature and gave 14% yield of aromatic monomers in the decomposition of organosolv lignin at 170 °C for 12 h. Subsequently, the same group [24] declared that the addition of NaOH to NiAu system can result in an enchanted selectivity towards aromatic compounds and inhibition for arene hydrogenation, and thus improve the reactivity for C–O bond hydrogenolysis both in model chemicals and real lignin. Specifically, the total monomer yield in the conversion of lignin increased from 7.6% to 10.9% at 160 °C for 4 h. Additionally, ZrO_2 supported PdNi bimetallic catalyst have been developed to selectively cleave β-O-4 linkage under ambient H_2 pressure, and exhibited enhanced activity compared with single Ni and Pd catalysts [22].

Despite the great advances, it is still urgent to develop more active and selective catalysts for aryl ether C–O bond cleavages of model chemicals and even in real lignin. AuPd bimetallic catalysts have been extensively studied and presented strong synergistic effect for many liquid-phase reactions, such as benzyl alcohol oxidation [25], levulinic acid hydrogenation [26], and dehydrogenation of HCOOH [27–30]. However, no literature have been reported regarding aryl ether C–O bond cleavage of lignin.

Besides H_2 as hydrogen source, formic acid is a cheap and alternative one because it abundantly comes from biomass with low toxicity and stability, offers H_2 very rapidly, and is safely handled in usage and storage [31–33]. Therefore, in this work the AuPd bimetallic catalysts fabricated by sol-immobilization method are employed to perform hydrogenolysis of lignin and derived model chemicals with formic acid. Their alloy structure was well characterized by TEM, XPS, UV–vis, and CO-DRIFTS. Remarkable enhancement in activity was observed for AuPd alloy in comparison to individual counterparts. More importantly, Au_1Pd_1/CeO_2 presented outstanding selectivities for hydrogenolysis of aryl ether C–O bond in both lignin and model compounds under mild conditions.

2. Materials and methods

2.1. Catalyst preparation

CeO_2 was prepared by a hydrothermal method described previously [34]. 4.5 mmol $Ce(NO_3)_3{\cdot}6H_2O$ (Sinopharm Chemical Reagent Co., Ltd. (SCRC)) was added into 90 mL NaOH solution (6 mol/L) under vigorous stirring at room temperature for 10 min. Subsequently, the mixture was transferred into an autoclave and hydrothermally treated at 100 °C for 24 h. After that, the precipitates were separated by centrifugation, dried at 80 °C overnight, and calcined at 400 °C for 4 h in static air.

The bimetallic Au_xPd_y/CeO_2 (x, y = 1, 3, where x and y stand for the molar ratio of Au with Pd in theory) was synthesized by sol-immobilization method [35,36]. Typically, 1 wt.% poly(vinyl alcohol) (PVA, Aladdin) solution was dissolved into the mixed aqueous solution of $PdCl_2$ (SCRC) and $HAuCl_4{\cdot}3H_2O$ (SCRC) with desired concentrations. Subsequently, 0.1 mol/L freshly prepared $NaBH_4$ solution (SCRC, $NaBH_4$/metal (molar ratio) = 5) was dripped to obtain a dark-brown sol under vigorous stirring for 30 min. The required amount of CeO_2 was added and continued to stir 5 h. After that, the precipitates were collected by centrifugation and dried at 80 °C overnight. The monometallic Au/CeO_2 and Pd/CeO_2 were prepared with similar method as above. The total noble metal content was controlled at ca. 2 wt.% in all the catalysts, and their actual compositions are listed in Fig. S1 in Supporting Information.

2.2. Catalyst characterization

N_2 adsorption − desorption isotherms were performed at −196 °C on a Micromeritics TriStar 3000 instrument. The samples were first evacuated under vacuum at 250 °C for 8 h prior to the measurements. X-ray diffraction (XRD) was performed on a Rigaku MiniFlex II desktop X-ray diffractometer operating with Cu Kα radiation at 40 kV and 40 mA at a scanning speed (2θ) of 4°/min. Transmission electron microscopy (TEM) and high-resolution TEM (HRTEM) were measured on a JEM-2011 F system electron micro-scope at 200 kV with a field emission gun. The sample was first suspended in ethanol under severe ultrasonication conditions for 20 min, and then deposited on copper grids coated with carbon foil. Metal dispersion has been estimated according to reported equation $D = 6 \times (v_m/a_m)/d$ [26], where v_m is the atomic density of Au (16.94×10^{-3} nm^3) or Pd (14.7×10^{-3} nm^3), a_m is the surface area for an atom of Au (8.75×10^{-2} nm^2) or Pd (7.93×10^{-2} nm^2), and d refers to the particle size based on TEM statistic. X-ray photoelectron spectroscopy (XPS) was obtained under an ultrahigh vacuum on a VG MiltiLab 2000 spectrometer equipped with Mg Kα radiation and a multichannel detector. The binding energies were calibrated by setting C1s peak to 284.6 eV. UV–vis spectra were collected on a Cary 5000 UV–vis-NIR spectrophotometer with $BaSO_4$ as a reference. H_2 temperature-programed desorption (H_2-TPD) was conducted in Auto Chem.II2920 apparatus (Mircromeritics, USA). Typically, 0.1 g fresh sample was pretreated in flowing 10 vol% H_2/Ar mixed gas at 250 °C for 60 min. When the system temperature was reduced to 50 °C, the sample was saturated with flowing H_2. Subsequently, the sample was heated to 500 °C at a ramp of 5 °C/min and the desorbed H_2 was monitored by a TCD detector. Diffuse reflectance infrared Fourier transform spectroscopy (DRIFTS) of CO adsorption was performed in a Nicolet iS10 spectrometer equipped with a MCT detector cooled with liquid N_2. The sample was first pretreated at 200 °C for 120 min in flowing Ar (20 mL/min). When the system was cooled to 25 °C, the sample was exposed to 10% v/v CO/Ar (20 mL/min) mixed gas until its saturation. Subsequently, the desorbed CO was recorded in flowing Ar again. Inductively coupled plasma optical emission spectroscopy (ICP) (Optima2100DV, PerkinElmer) was employed to determine the metal contents of as-prepared catalysts.

2.3. Catalytic test

The organosolv lignin was extracted from typical hardwood locust according to the reported method [37]. The locust sawdust was supplied by a local manufactory (ca. 40 mesh), and dried at 100 °C for 1 day before its use. 1.0 g locust sawdust, 30 mL ethanol and 30 mL water were charged into an autoclave. The reactor was heated to 180 °C and kept for 5 h. Subsequently, the reaction system was cooled down in an ice-water bath. A reddish-brown solution was separated by centrifugation, and the solvent was removed by a rotary evaporator. Finally, the collected lignin was dried at 100 °C overnight.

All the reactions were carried out in a 50 mL Teflon-lined stainless steel autoclave. Typically, 0.2 mmol feed or 0.03 g organosolv lignin, 15 mL H_2O, 2 mmol or 10 mmol formic acid and 0.1 g catalyst were loaded into the reactor. The reaction was performed at preset temperature for desired time under vigorous stirring. After the completion of reaction, the reactor was quickly cooled to room temperature in an ice-water bath. The products were collected by centrifugation, extracted by ethyl acetate, and analyzed by gas chromatography (Shimadzu GC-2010) with a flame ionization detector using a DB-1 capillary column. Ethyl benzoate was used as an internal standard. The assignments of products were determined by GC–MS. The quantitative analysis was estimated by the following equations:

$$\text{Conversion}(\%) = \frac{\text{moles of initial reactant} - \text{moles of remained reactant}}{\text{moles of initial reactant}} \times 100$$

$$\text{Selectivity}(\%) = \frac{\text{moles of one product}}{\text{moles of all products}} \times 100$$

The concentrations of formic acid were analyzed by HPLC (Agilent 1100 Series) using UV–vis detector and an Eclipse XDB-C18 column. The mobile phase was 0.005 mol/L H_2SO_4 flowing at a rate of 1.0 mL/min. The column oven was set at 30 °C. For lignin depolymerization, the product yield was defined as the mass of monophenol divided by the mass of lignin.

3. Results and discussion

3.1. Catalyst characterization

The PVA capped AuPd bimetallic nanoparticles were prepared by the co-reduction of $PdCl_2$ and $HAuCl_4$ by $NaBH_4$, and subsequently deposited on rod-shaped CeO_2 support. The composition of AuPd nanoparticles can be regulated by the initial molar ratio of their precursors and analyzed by ICP. The metal contents and textural properties are listed in Table S1. All the samples displayed similar BET surface area and pore distributions. As illustrated in Fig. S1, the typical diffuse diffraction peaks around 28.8°, 33.3°, 47.8° and 56.5° were ascribed to face-centered-cubic (fcc) structure of CeO_2 [38]. Only weak Au diffraction peak at 38.4° were detected over Au/CeO_2 while no Pd-containing peaks were observed, probably due to the high Pd dispersion or low metal content. The representative TEM micrographs and particle size distribution histograms for the $AuPd/CeO_2$ catalysts are illustrated in Fig. 1. In all the samples, the CeO_2 primarily presented as disordered rod shape, consistent with previous result [34]. Au nanoparticles proceeded to agglomeration and some of them were larger than 10 nm in size over Au/CeO_2. Pd nanoparticles were distributed uniformly on the CeO_2 surface with a 6.4 nm average particle size over Pd/CeO_2. The corresponding lattice fringes in HRTEM confirmed the presence of crystalline Pd nanoparticles. All the bimetallic AuPd samples showed highly dispersed nanoparticles and lower particle size compared to the monometallic samples. In addition, the AuPd species form an extended flat interface structure with rod-shaped crystalline ceria surface, suggesting that AuPd nanoparticles are tightly attached on CeO_2 surface. The HRTEM image of bimetallic AuPd nanoparticles are indicative of polycrystalline face-centered cubic (fcc) structure with exposed {1 1 1} lattice fringes measured to be 0.227 nm, which is lower than that of fcc Au (0.235 nm) and larger than the {1 1 1} spacing of fcc Pd (0.221) [39]. This is probably related to the formation of alloy structure.

The formation of AuPd alloy structure for the bimetallic samples can also be verified by XPS, UV–vis spectra and CO-DRIFTS. As displayed in Fig. 2a of XPS spectra, Au/CeO_2 exhibited spin-orbit split peaks centered at 83.7 and 87.3 eV, which were assigned to Au $4f_{7/2}$ and Au $4f_{5/2}$ of metallic Au, respectively [34]. Compared to Au/CeO_2, the addition of Pd induced the movement of Au 4f peaks towards low binding energy, suggesting that Au species were in the electron-rich states. Two peaks at around 334.7 and 339.9 eV were detected over Pd/CeO_2, corresponding to metallic Pd [26]. The Pd 3d peaks shifted to high binding energy because of Au incorporation over AuPd bimetallic catalysts. There is strong electronic interaction between Au and Pd owing to alloy effect, wherein the electrons transfer from Pd to Au. The surface ratio of Au and Pd was estimated to be 1.2 by XPS peak area, similar to that of bulk phase in Au_1Pd_1/CeO_2, indicating that Au and Pd atoms were homogenously distributed in AuPd alloy structure. As illustrated in Fig. 2c for UV–vis spectra, Au/CeO_2 exhibited characteristic surface plasmon resonance (SPR) adsorption at 520 nm while Pd/CeO_2 did not have any SPR adsorption [39]. After the addition of Pd into Au/CeO_2, the SPR adsorption of Au declined sharply and even completely disappeared owing to the alloy effect.

CO-DRIFTS were performed to probe electronic effect and the results are illustrated in Fig. 2d. Au/CeO_2 exhibited only one carbonyl stretching peak at 2114 cm^{-1}, corresponding to linear adsorption of CO on Au [40]. The intense two peaks were observed at around 2083 and 1923 cm^{-1}, which were assigned to linear and bridged adsorption of CO on Pd [40], respectively. Notably, the linear adsorption of CO located at the corner of edges sites of undercoordinated Pd, while bridged CO adsorption located on surface Pd. These two peaks presented a similar change in intensity on $AuPd/CeO_2$, strongly indicating that Au and Pd species were homogenously dispersed and didn't form core-shell structure, consistent well with HRTEM results. Moreover, the adsorption peaks of CO displayed an obvious blue-shift with increasing Au content, suggesting strong electronic interaction between Au and Pd species. According to d-π model [40], Au electron density increases from Pd donation during the formation of AuPd alloy.

H_2-TPD was conducted to reflect the adsorption of H_2 on active metallic surface (Fig. 3). Au/CeO_2 displayed two weak H_2 desorption peaks at around 80 and 425 °C, reflecting that H_2 is not easily adsorbed and activated on Au surface. Compared to Au/CeO_2, AuPd alloy catalysts obviously improve adsorption capacity of H_2. Similar H_2 desorption peaks were observed over Pd/CeO_2, suggesting that the adsorption strength of H_2 is similar with AuPd bimetallic catalysts. Moreover, Pd/CeO_2 showed two strong peaks at around 80 and 365 °C, and possessed the highest adsorption capacity of H_2.

3.2. Hydrogenolysis of benzyl phenyl ether (α-O-4) with formic acid

The catalytic performance was initially evaluated with model compounds benzyl phenyl ether, 2-phenylethyl phenyl ether and diphenyl ether to mimic α-O-4, β-O-4 and 4-O-5 of lignin, respectively. As listed in Table 1, only 3.5% conversion of benzyl phenyl ether and 40.1% conversion of formic acid were obtained over Au/CeO_2 at 150 °C for 1 h. Because the amount of formic acid far exceeds that of benzyl phenyl ether, the low conversion of Au/CeO_2 is not predominantly ascribed to the lack of hydrogen donor. Pd/CeO_2 gave 49.6% conversion of benzyl phenyl ether and 76.3% conversion of formic acid. Compared to Au/CeO_2 and Pd/CeO_2, all the bimetallic AuPd catalysts displayed excellent activity of benzyl phenyl ether and complete conversion of formic acid. Of them, Au_1Pd_1/CeO_2 exhibited the highest reactivity and reached 100% conversions of benzyl phenyl ether and formic acid. Moreover, the conversion of benzyl phenyl ether over Au_1Pd_1/CeO_2 was much higher than that of mixed catalyst Au/CeO_2 + Pd/CeO_2, suggesting that there was remarkable synergistic effect between bimetallic species. Regarding the selectivity, all the samples gave similar product distributions with good C–O bond cleavage ability. 41.8% phenol and 52.4% toluene were achieved over Au_1Pd_1/CeO_2. Kinetic analysis in Fig. S2 displays the correlation between reaction rate with benzyl phenyl ether and formic acid concentration, respectively. The reaction orders with respect to benzyl phenyl ether and formic acid concentration were calculated to be 0.69 and 0.14, respectively. Thus, the higher reaction order of benzyl phenyl ether indicates that C–O bond cleavage is the rate-determining step.

Turnover frequency (TOF) can be employed to reflect the intrinsic

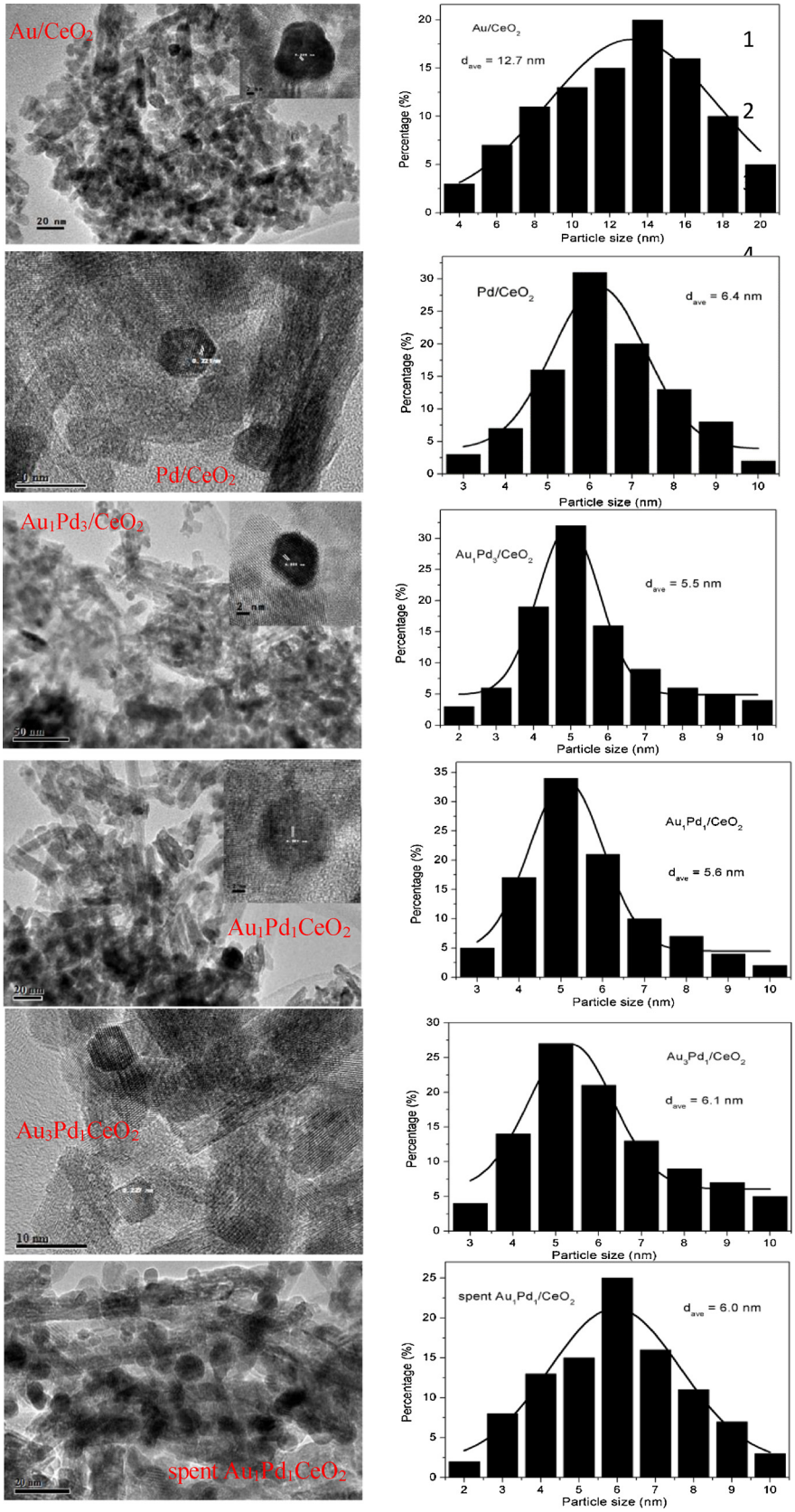

Fig. 1. TEM images and corresponding metal particle size distribution histograms as well as the inserted HRTEM images at the upper right corner.

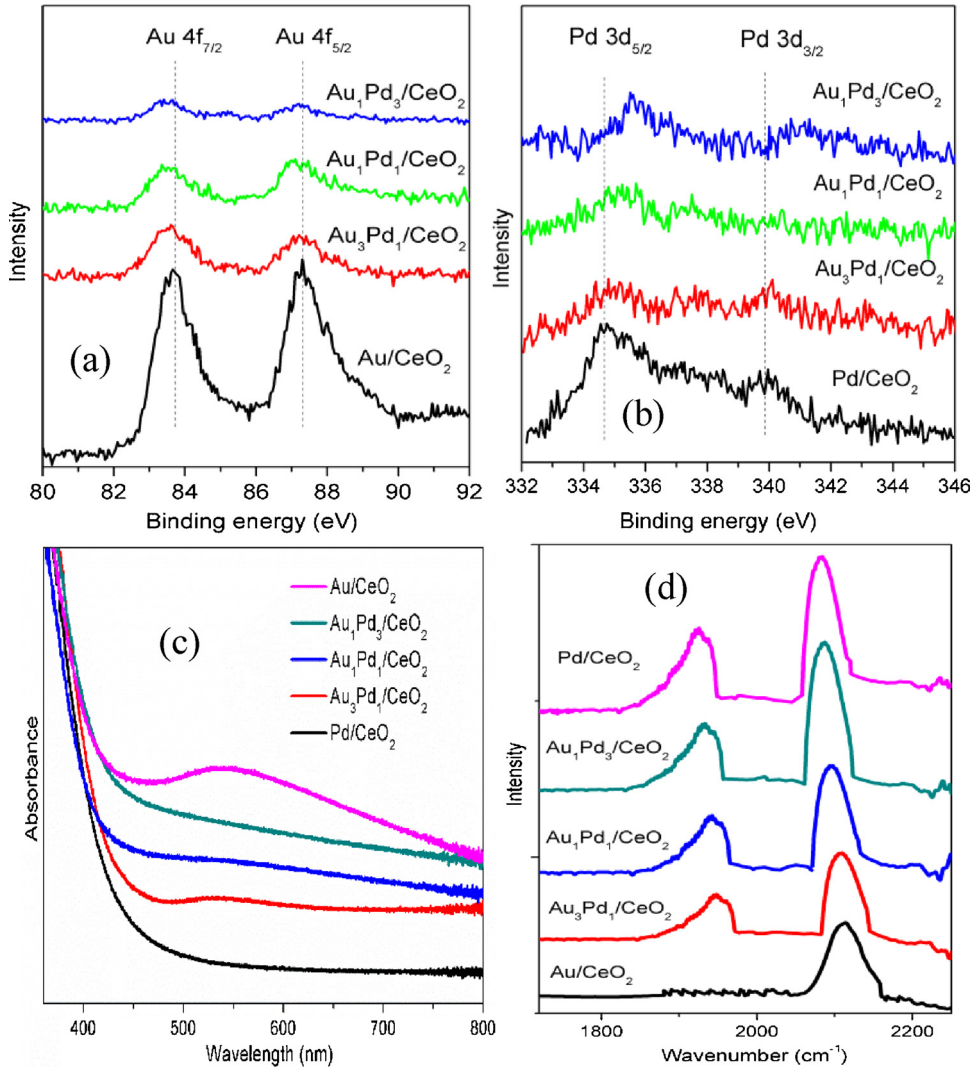

Fig. 2. (a) Au 4f and (b) Pd 3d XPS spectra, (c) UV–vis spectra and (d) CO-DRIFTS over various catalysts.

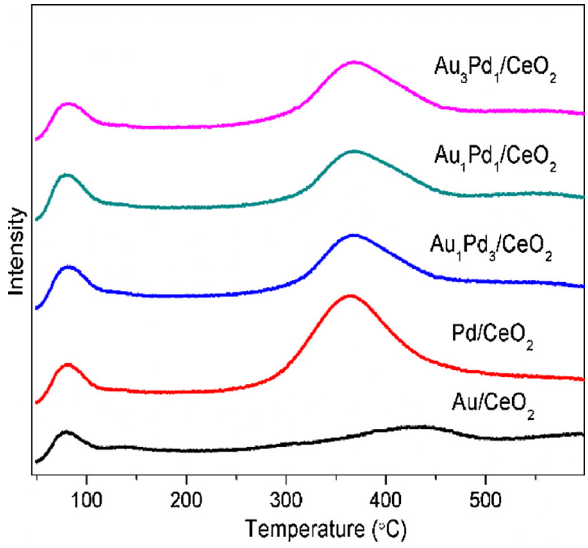

Fig. 3. H_2-TPD profiles of different catalysts.

Table 1
Hydrogenolysis of benzyl phenyl ether (α-O-4) over different catalysts[a].

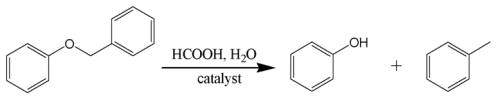

Catalyst	Conversion (%)		Selectivity (%)		TOF[b] (h^{-1})
	benzyl phenyl ether	HCOOH	phenol	toluene	
Au/CeO_2	3.5	40.1	47.8	51.3	7.5
Pd/CeO_2	49.6	76.3	45.3	52.6	29.5
Au_1Pd_3/CeO_2	90.4	100	44.9	50.8	121.0
Au_1Pd_1/CeO_2	100	100	41.8	52.4	176.3
Au_3Pd_1/CeO_2	89.6	100	43.5	53.9	83.0
Au/CeO_2 + Pd/CeO_2[c]	51.2	95.2	46.1	50.7	23.9

[a] Reaction conditions: 0.2 mmol benzyl phenyl ether, 2 mmol formic acid, 150 °C, 1 h, 0.1 g catalyst.
[b] TOF is moles of converted feed per mole of surface metal sites and per hour. Reaction conditions were chosen to determine the rate below 20% conversion.
[c] 0.1 g Au/CeO_2 + 0.1 g Pd/CeO_2.

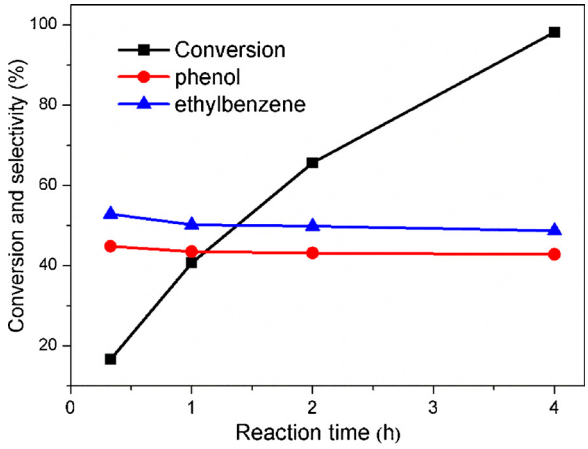

Fig. 4. The effect of reaction time on the hydrogenolysis of 2-phenylethyl phenyl ether (β-O-4) over Au_1Pd_1/CeO_2. Reaction conditions: 0.2 mmol 2-phenylethyl phenyl ether, 2 mmol formic acid, 150 °C, 1 h, 0.1 g Au_1Pd_1/CeO_2.

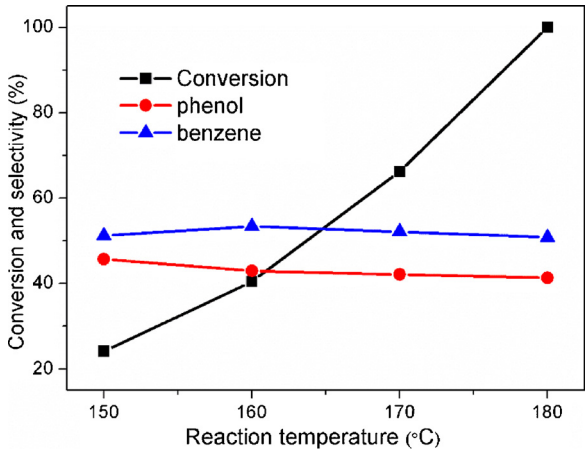

Fig. 5. Effect of reaction temperature on the hydrogenolysis of diphenyl ether (4-O-5) over Au_1Pd_1/CeO_2. Reaction conditions: 0.2 mmol diphenyl ether, 2 mmol formic acid, 24 h, 0.1 g Au_1Pd_1/CeO_2.

Table 2
Comparison of the model compounds.

Linkage	Model compound	BDE[a] (kJ/mol)	TOF (h^{-1})
α-O-4	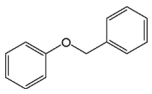	218	176.3
β-O-4	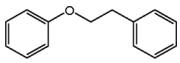	289	36.8
4-O-5	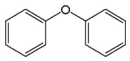	314	0.74

[a] Data was obtained from the reported reference [5].

reactive ability and the results are listed in Table 1. The TOF based on accessible surface metallic atoms of Au_1Pd_1/CeO_2 was estimated to be 176.3 h^{-1}, and this value is 23.5-fold and 6-fold increase in activity compared with Au/CeO_2 and Pd/CeO_2, respectively. The significant improvement of intrinsic activity of Au_1Pd_1/CeO_2 can not be randomly ascribed to nano size effect, because no discernable decrease in size was observed in comparison with Pd/CeO_2. As can be seen from H_2-TPD result, Pd/CeO_2 possesses much more H_2 adsorption capacity and similar adsorption strength in comparison to AuPd bimetallic catalysts, indicating that the adsorption and activation of H_2 from HCOOH release is not the rate-determining step. Moreover, the higher reaction order of benzyl phenyl ether confirms that the activation ability of α-O-4 bond is the key factor in determining the catalytic performance. Electronic and geometric effects of AuPd bimetallic species are thought to be responsible for the superior catalytic performance owing to the formation of alloy structure. Based on XPS, UV–vis, CO-FTIR and earlier report [8], the electron-deficient Pd facilitates the strong adsorption of electron-rich α-O-4 bond of benzyl phenyl ether, thus weakening its α-O-4 bond. Meanwhile, the activated H* over AuPd surface can further attack α-O-4 bond and promote the cleavage of α-O-4 bond. Regarding geometric effect, previous DFT calculations indicate that the incorporation of larger Au atoms into Pd lattice leads to lattice mismatch and tensile strain [41]. The narrowing and upward shift in d-band of Pd because of tensile strain can form more coordinatively unsaturated sites for surface atoms, and enhances the cleavage for α-O-4 bond.

3.3. Hydrogenolysis of 2-phenylethyl phenyl ether (β-O-4) and diphenyl ether (4-O-5) with formic acid over Au_1Pd_1/CeO_2

Since Au_1Pd_1/CeO_2 catalyst exhibits the best catalytic performance, it is chosen as the system catalyst to perform hydrogenolysis of β-O-4 and 4-O-5 bonds. As described in Fig. 4, the initial conversion of 2-phenylethyl phenyl ether was 40.7% for 1 h, and then increased to 98.2% for 4 h. Additionally, the β-O-4 bond of 2-phenylethyl phenyl ether was selectively cleaved into phenol and ethylbenzene. Regarding 4-O-5 bond (Fig. 5), the conversion of diphenyl ether was only 24.1% at 150 °C for 24 h, suggesting that the aromatic ether C–O bond is hardly to cleave. The conversion of diphenyl ether increased to 40.4% at 160 °C, and reached 100% with increasing temperature at 180 °C. The predominant products were phenol and benzene, originating from the selective cleavage of 4-O-5 bond. Their total selectivities declined from 96.9% to 92.1% in the temperature range from 160 to 180 °C due to the formation of alkanes byproducts.

We have systematically compared the C–O bond cleavage activity for α-O-4, β-O-4 and 4-O-5 bonds. As shown in Table 2, the TOF of α-O-4 bond is much higher than 36.8 h^{-1} obtained for β-O-4 bond. Additionally, the TOF value of 4-O-5 bond is only 0.74 h^{-1}, confirming that 4-O-5 bond is the most recalcitrant one to cleave in lignin. Bond-dissociation energy (BDE) is an important parameter to determine the strength of the C–O ether bond [5]. As displayed in Table 2, the BDE of aryl ether bond 4-O-5 (314 kJ mol^{-1}) is much higher than that of aliphatic ether bonds of α-O-4 (218 kJ mol^{-1}) and β-O-4 (289 kJ mol^{-1}). It can be seen that the higher the BDE is, the lower the TOF will be. Thus, based on our reaction results and BDE, the strength of C–O ether bond is decreased in the following order: 4-O-5 > β-O-4 ≥ α-O-4, consistent well with previous results [5].

3.4. Reusability test

To explore the reusability behavior, the spent Au_1Pd_1/CeO_2 catalyst was separated from the reaction mixture by centrifugation. As displayed in Fig. 6a, both benzyl phenyl ether conversion and product distributions did not present obvious decline during five reaction cycles. Because the deactivation of catalyst may be masked at complete conversion of benzyl phenyl ether, the recycling tests were further performed for robust 4-O-5 bond at low conversion. Similar case (Fig. 6b) was observed that the conversion of diphenyl ether and the product distribution was maintained within five runs. The TEM image (Fig. 1) of spent Au_1Pd_1/CeO_2 confirmed that the agglomeration of AuPd nanoparticles did not occur owing to the strong electronic interaction of AuPd alloy.

3.5. Hydrogenolysis of lignin with formic acid over Au_1Pd_1/CeO_2

As evidenced above, the Au_1Pd_1/CeO_2 catalyst with formic acid system has been proved very efficient for the cleavage of dimeric model

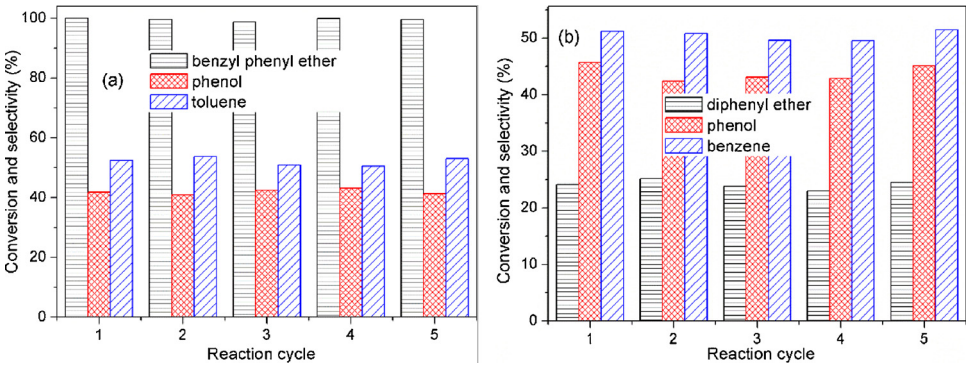

Fig. 6. (a) Reusability tests for hydrogenolysis of benzyl phenyl ether. Reaction conditions: 0.2 mmol benzyl phenyl ether, 2 mmol formic acid, 150 °C, 1 h, 0.1 g Au_1Pd_1/CeO_2. (b) Reusability tests for hydrogenolysis of diphenyl ether. Reaction conditions: 0.2 mmol diphenyl ether, 2 mmol formic acid, 150 °C, 24 h, 0.1 g Au_1Pd_1/CeO_2.

Table 3
Depolymerization of organosolv lignin with formic acid over Au_1Pd_1/CeO_2.[a].

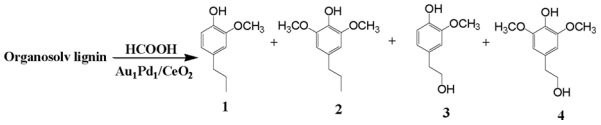

Temperature (°C)	Yield (%)				Total monophenols yield (%)
	1	2	3	4	
160	2.7	13.5	1.0	0.6	27.0
180	4.3	19.4	3.1	1.3	44.1
200	3.2	18.8	1.0	1.1	34.7
220	1.2	15.0	1.1	1.1	31.5

[a] Reaction conditions: 0.03 g lignin, 10 mmol formic acid, 6 h, 0.1 g Au_1Pd_1/CeO_2.

compounds, which mimic the various C–O bonds in lignin. Inspired by the good results of model compound hydrogenolysis, we applied this elegant strategy to disassemble actual hardwood locust lignin. The depolymerization of lignin resulted in a variety of valuable monophenols, mainly including 4-*n*-propylguaiacol (**1**), 4-*n*-propylsyringol (**2**), 4-*n*-propanolguaiacol (**3**), and 4-*n*-propanolsyringol (**4**). The detailed product distributions for the identified monophenols are described in Table S2. As listed in Table 3, the total yield of monophenols mounted to 27.0% at 160 °C, and reached 44.1% at 180 °C. However, the yield gradually declined to 31.5% with increasing temperature to 220 °C owing to the formation of some repolymerization products. Despite the recalcitrant structure, our formic acid-mediated Au_1Pd_1/CeO_2 alloy catalyst has effectively converted lignin into aromatic monomer with good yield at low temperature. In the presence of promotional NaOH, the previous NiAu bimetallic catalyst obtained only 10.9% yield of total monomer in the hydrogenolysis of organosolv lignin at 160 °C and 10 bar H_2 [24]. Notably, the structure of lignin varies with different sources, which may affect the final product distribution [2]. Even so, our monomer yield of 44.1% is higher than most of the previous results under low reaction temperature [8,42–46]. Thus, our AuPd alloy provides an excellent example in the design of advanced nanocatalyst for biomass utilization [47].

4. Conclusions

We have successfully fabricated Au_1Pd_1/CeO_2 alloy catalyst with an exceptionally high activity for aryl ether C–O bond cleavage, almost one order of magnitude higher than its single metal counterparts. AuPd alloy resulted in strong electronic interactions between Au and Pd atoms. The decrease in the electron density of Pd sites remarkably increased the adsorption capacity for aromatic C–O bond, and greatly improve reaction rate. More importantly, a variety of valuable monophenols can be directly produced from lignin over Au_1Pd_1/CeO_2 with formic acid, reaching 44.1% yield under relatively mild conditions. This provides a powerful approach for the production of aromatic chemicals from lignin hydrogenolysis without high-pressure hydrogen. It's anticipated that these monophenols can be facilely upgraded into bio-oils via hydrodeoxygenation, which is currently investigated in our lab.

Acknowledgements

This work is financially supported by National Natural Science Foundation of China (21878321), Youth Innovation Promotion Association CAS (2015140), Natural Science Foundation of Shanxi Province (2016021033), and Science Foundation for Youth Scholars of State Key Laboratory of Coal Conversion (2016BWZ002).

Appendix A. Supplementary data

Supplementary material related to this article can be found, in the online version, at doi:https://doi.org/10.1016/j.mcat.2018.10.022.

References

[1] C. Li, X. Zhao, A. Wang, G.W. Huber, T. Zhang, Chem. Rev. 115 (2015) 11559–11624.
[2] S. Zhu, J. Guo, X. Wang, J. Wang, W. Fan, ChemSusChem 10 (2017) 2547–2559.
[3] C. Xu, R.A.D. Arancon, J. Labidi, R. Luque, Chem. Soc. Rev. 43 (2014) 7485–7500.
[4] A.J. Ragauskas, G.T. Beckham, M.J. Biddy, R. Chandra, F. Chen, M.F. Davis, B.H. Davison, R.A. Dixon, P. Gilna, M. Keller, P. Langan, A.K. Naskar, J.N. Saddler, T.J. Tschaplinski, G.A. Tuskan, C.E. Wyman, Science 344 (2014) 709.
[5] J. He, C. Zhao, J.A. Lercher, J. Am. Chem. Soc. 134 (2012) 20768–20775.
[6] V. Molinari, C. Giordano, M. Antonietti, D. Esposito, J. Am. Chem. Soc. 136 (2014) 1758–1761.
[7] J. Lu, M. Wang, X. Zhang, A. Heyden, F. Wang, ACS Catal. 6 (2016) 5589–5598.
[8] J. Zhang, J. Teo, X. Chen, H. Asakura, T. Tanaka, K. Teramura, N. Yan, ACS Catal. 4 (2014) 1574–1583.
[9] X. Besse, Y. Schuurman, N. Guilhaume, Appl. Catal. B: Environ. 209 (2017) 265–272.
[10] J. Zhang, H. Asakura, J. van Rijn, J. Yang, P. Duchesne, B. Zhang, X. Chen, P. Zhang, M. Saeys, N. Yan, Green Chem. 16 (2014) 2432–2437.
[11] A.G. Sergeev, J.F. Hartwig, Science 332 (2011) 439–443.

[12] J.M. Nichols, L.M. Bishop, R.G. Bergman, J.A. Ellman, J. Am. Chem. Soc. 132 (2010) 12554–12555.
[13] Y. Ren, M. Yan, J. Wang, Z.C. Zhang, K. Yao, Angew. Chem. Int. Ed. 52 (2013) 12674–12678.
[14] R.R. Barton, M. Carrier, C. Segura, J.L.G. Fierro, S. Park, H.H. Lamb, N. Escalona, S.W. Peretti, Appl. Catal. A Gen. 562 (2018) 294–309.
[15] J. He, C. Zhao, D. Mei, J.A. Lercher, J. Catal. 309 (2014) 280–290.
[16] M. Zaheer, J. Hermannsdörfer, W.P. Kretschmer, G. Motz, R. Kempe, ChemCatChem 6 (2014) 91–95.
[17] Y. Hu, G. Jiang, G. Xu, X. Mu, Mol. Catal. 445 (2018) 316–326.
[18] T.H. Parsell, B.C. Owen, I. Klein, T.M. Jarrell, C.L. Marcum, L.J. Haupert, L.M. Amundson, H.I. Kenttamaa, F. Ribeiro, J.T. Miller, M.M. Abu-Omar, Chem. Sci. 4 (2013) 806–813.
[19] J. Li, H. Sun, J.-x. Liu, J.-j. Zhang, Z.-x. Li, Y. Fu, Mol. Catal. 452 (2018) 36–45.
[20] J.K. Kim, J.K. Lee, K.H. Kang, J.W. Lee, I.K. Song, J. Mol. Catal. A Chem. 410 (2015) 184–192.
[21] J.K. Kim, J.K. Lee, K.H. Kang, J.C. Song, I.K. Song, Appl. Catal. A Gen. 498 (2015) 142–149.
[22] J.-w. Zhang, Y. Cai, G.-p. Lu, C. Cai, Green Chem. 18 (2016) 6229–6235.
[23] A.L. Jongerius, R. Jastrzebski, P.C.A. Bruijnincx, B.M. Weckhuysen, J. Catal. 285 (2012) 315–323.
[24] H. Konnerth, J. Zhang, D. Ma, M.H.G. Prechtl, N. Yan, Chem. Eng. Sci. 123 (2015) 155–163.
[25] H. Wang, C. Wang, H. Yan, H. Yi, J. Lu, J. Catal. 324 (2015) 59–68.
[26] W. Luo, M. Sankar, A.M. Beale, Q. He, C.J. Kiely, P.C.A. Bruijnincx, B.M. Weckhuysen, Nature Commun. 6 (2015) 6540.
[27] P. Stathi, Y. Deligiannakis, G. Avgouropoulos, M. Louloudi, Appl. Catal. A Gen. 498 (2015) 176–184.
[28] D.A. Bulushev, M. Zacharska, S. Beloshapkin, Y. Guo, I. Yuranov, Appl. Catal. A Gen. 561 (2018) 96–103.
[29] D.A. Bulushev, S. Beloshapkin, P.E. Plyusnin, Y.V. Shubin, V.I. Bukhtiyarov, S.V. Korenev, J.R.H. Ross, J. Catal. 299 (2013) 171–180.
[30] W.-Y. Yu, G.M. Mullen, D.W. Flaherty, C.B. Mullins, J. Am. Chem. Soc. 136 (2014) 11070–11078.
[31] A. Bulut, M. Yurderi, Y. Karatas, M. Zahmakiran, H. Kivrak, M. Gulcan, M. Kaya, Appl. Catal. B: Environ. 164 (2015) 324–333.
[32] M. Grasemann, G. Laurenczy, Energy Environ. Sci. 5 (2012) 8171–8181.
[33] Z. Li, Q. Xu, Acc. Chem. Res. 50 (2017) 1449–1458.
[34] S. Zhu, Y. Xue, J. Guo, Y. Cen, J. Wang, W. Fan, ACS Catal. 6 (2016) 2035–2042.
[35] L. Kesavan, R. Tiruvalam, M.H.A. Rahim, M.I. bin Saiman, D.I. Enache, R.L. Jenkins, N. Dimitratos, J.A. Lopez-Sanchez, S.H. Taylor, D.W. Knight, C.J. Kiely, G.J. Hutchings, Science 331 (2011) 195–199.
[36] G.L. Brett, P.J. Miedziak, N. Dimitratos, J.A. Lopez-Sanchez, N.F. Dummer, R. Tiruvalam, C.J. Kiely, D.W. Knight, S.H. Taylor, D.J. Morgan, A.F. Carley, G.J. Hutchings, Catal. Sci. Technol. 2 (2012) 97–104.
[37] P. Ferrini, R. Rinaldi, Angew. Chem. Int. Ed. 53 (2014) 8634–8639.
[38] S. Zhu, X. Gao, Y. Zhu, Y. Li, Green Chem. 18 (2016) 782–791.
[39] O. Metin, X. Sun, S. Sun, Nanoscale 5 (2013) 910–912.
[40] J.H. Carter, S. Althahban, E. Nowicka, S.J. Freakley, D.J. Morgan, P.M. Shah, S. Golunski, C.J. Kiely, G.J. Hutchings, ACS Catal. 6 (2016) 6623–6633.
[41] M. Mavrikakis, B. Hammer, J.K. Nørskov, Phys. Rev. Lett. 81 (1998) 2819–2822.
[42] A. Toledano, L. Serrano, A. Pineda, A.A. Romero, R. Luque, J. Labidi, Appl. Catal. B: Environ. 145 (2014) 43–55.
[43] P. Chen, Q. Zhang, R. Shu, Y. Xu, L. Ma, T. Wang, Bioresour. Technol. Rep. 226 (2017) 125–131.
[44] M.J. Hidajat, A. Riaz, J. Park, R. Insyani, D. Verma, J. Kim, Chem. Eng. J. 317 (2017) 9–19.
[45] S. Jeong, S. Yang, D.H. Kim, Mol. Catal. 442 (2017) 140–146.
[46] M. Verziu, A. Tirsoaga, B. Cojocaru, C. Bucur, B. Tudora, A. Richel, M. Aguedo, A. Samikannu, J.P. Mikkola, Mol. Catal. 450 (2018) 65–76.
[47] Y. Wang, S. De, N. Yan, Chem. Commun. (Camb.) 52 (2016) 6210–6224.